Cross-organ Analysis Reveals Associations between Vascular Properties of the Retina, the Carotid and Aortic Artery, and the Brain

Sofía Ortín Vela[†][1,2] and Sven Bergmann[†][1,2,3]

[1]Department of Computational Biology, University of Lausanne, Lausanne, Switzerland
[2]Swiss Institute of Bioinformatics, Lausanne, Switzerland
[3]Department of Integrative Biomedical Sciences, University of Cape Town, Cape Town, South Africa

Abstract

Vascular properties of the retina are not only indicative of ocular but also systemic cardio- and cerebrovascular health. Yet, the extent to which retinal vascular morphology reflects that in other organs is not well understood. We used morphological vascular phenotypes derived from the brain, the carotid artery, the aorta, and the retina from the UK Biobank, with sample sizes between 18,808 and 68,000 subjects per phenotype. We examined the cross-organ phenotypic and genetic correlations, as well as common associated genes and pathways. White matter hyperintensities positively correlated with carotid intima-media thickness, lumen diameter, and aortic cross-sectional areas but negatively correlated with aortic distensibility. Retinal vascular density showed negative correlations with white matter hyperintensities, intima-media thickness, lumen diameter, and aortic areas, while positively correlating with aortic distensibility. Significant correlations were also observed between other retinal phenotypes and white matter hyperintensities, as well as with aortic phenotypes. Correcting for hypertension reduced the magnitude of these correlations, but the overall correlation structure largely persisted. Genetic correlations and gene enrichment analyses identified potential regulators of these phenotypes, with some shared genetic influence between retinal and non-retinal phenotypes. Our study sheds light on the complex interplay between vascular morphology across different organs, revealing both shared and distinct genetic underpinnings. This highlights the potential of retinal imaging as a non-invasive prognostic tool for systemic vascular health.

Keywords: Vasculature, IDPs, GWAS, brain, carotid, IMT, LD, aorta, retina, hypertension, genes, pathways.

*E-mails: sofia.ortinvela@unil.ch, and sven.bergmann@unil.ch

Nonstandard Abbreviations and Acronyms

ASEG: Automatic subcortical segmentation

ASL: Arterial spin labeling

ATT: Arterial transit time

CBF: Cerebral blood flow

CFIs: Color fundus images

DBP: Diastolic blood pressure

FLAIR: Fluid-attenuated inversion recovery

IDP: Image-derived phenotype

IMT: Intima-media thickness

LD: Lumen diameter

LDSR: Linkage disequilibrium score regression

MRA: Magnetic resonance angiography

MRI: Magnetic resonance imaging

PC: Principal component

SBP: Systolic blood pressure

UKB: UK Biobank

WMH: White matter hyperintensities

1 Introduction

The vascular system is a complex network of blood vessels, including arteries, veins, and capillaries, essential for circulating blood throughout the body. This system plays a crucial role in delivering oxygen and nutrients to various tissues, removing waste products, and maintaining overall health. Blood flows from the heart through arteries, arterioles, and capillaries, then returns through venules and veins. Smaller arterioles branch out from the arteries and lead to the capillaries. Venules and veins return blood to the heart, acting as volume reservoirs and maintaining a pressure gradient crucial for blood circulation.

Simple physiological measures such as arterial blood pressure and blood oxygen saturation provide valuable insights into the functionality of the vascular system. However, medical imaging offers more detailed information specific to different vascular structures. Angiography, for example, provides high-resolution images of blood vessels, detecting occlusions or poorly perfused regions, but is typically used only when disease risk is suspected due to its invasive nature [1]. Non-invasive techniques like non-contrast magnetic resonance angiography (MRA) offer lower spatial resolution but are suitable for studies involving healthy subjects. Despite their non-invasive nature, these imaging modalities remain expensive [2]. In contrast, imaging of the retina vasculature is an inexpensive, non-invasive routine examination that can provide valuable insights into systemic vascular health [3].

Various studies have explored the associations between altered vascular morphology and vascular problems across different parts of the body. Increased arterial stiffness and greater carotid intima-media thickness (IMT) are known to elevate the risk of future hypertension and cardiovascular diseases [4]. Higher carotid IMT also correlates with atherosclerosis [4]. Increased carotid lumen diameter (LD) is independently associated with a higher risk of cardiovascular events [5, 6]. Abdominal aortic aneurysms, intracranial aneurysms, and coronary artery ectasia or aneurysms share similar pathophysiological mechanisms involving vascular dilation and remodeling [7]. The presence of arterial aneurysms across different vascular territories suggests a common underlying vascular wall pathology [7]. Aortic dimensions and distensibilities are critical risk factors for aortic aneurysms, and other cardio- and cerebrovascular diseases [8]. Also, changes in the retinal vasculature have been linked to vascular issues in distant organs, including stroke [9–11], coronary heart disease [12, 13], or hypertension [14, 15], indicating systemic associations.

Despite the ample evidence for associations of systemic vascular disease with single-organ vasculature morphology, the relationship between similar vascular morphological properties across different organs remains poorly understood. Although some studies have analyzed the phenotypic and genetic correlations between image-derived phenotypes (IDPs) of different organs such as the heart, brain, retina, and liver [16–19], they have not focused on the morphology of the vasculature itself. This study aims to shed light on these associations using data from the UK Biobank (UKB) [20, 21], which includes multiple vascular IDPs from the brain, carotid [22], heart [23–28], and retina [29, 30]. We investigated both phenotypic and genetic correlations between these IDPs, highlighting shared associated genes and pathways. Our approach reveals several relationships between vascular morphology across different organs, including the retina, emphasizing

its potential as a prognostic proxy for non-retinal vascular diseases.

2 Results

The UKB includes nearly 186,000 retinal color fundus images (CFIs) collected from approximately 90,000 subjects. We recently measured 17 different IDPs for 71,000 subjects whose CFIs passed quality control (QC) [30], utilizing some of these within this investigation. Additionally, we measured the carotid lumen diameter (LD) for 18,808 subjects (after QC) using ultrasound images of the UKB [22] and incorporated these measurements into our study. We searched for other reliable non-retinal vascular IDPs available for a substantial number of subjects (at least 1,000) and identified the following IDPs: white matter hyperintensities (WMH) from T2-weighted brain magnetic resonance imaging (MRI), measurements of carotid IMT from ultrasound images, and assessments of the cross-sectional area and distensibility of the ascending and descending aorta from cardiac MRI. After filtering, these measurements were available for approximately 40,000, 49,000, and 36,000 subjects, respectively (see Figure 1).

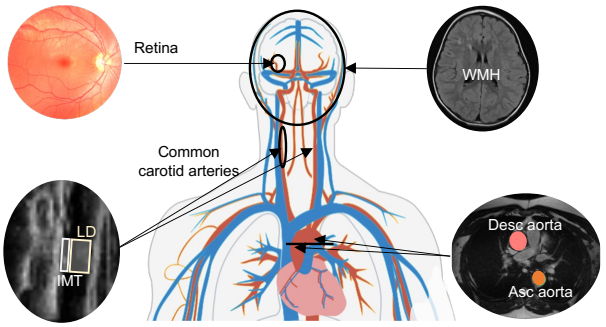

Figure 1: Visualization of the human vascular system and the imaging modalities available in the UKB. The modalities include CFIs for examining the retina's vasculature, ultrasound for assessing the common carotid arteries (in particular, the IMT and the LD), transverse cardiac MRI for evaluating the aorta, and structural brain MRI for detecting WMH.

For retinal IDPs, we selected tortuosity, vascular density, and vessel diameter, which are relatable to non-retinal IDPs used. Although retinal IDPs include both arteriolar and venular measurements, non-retinal IDPs focus mainly on arterial characteristics (see Supplementary Data 'IDPs information' for details).

2.1 Phenotypic and genetic correlations between vascular IDPs

We first adjusted all vascular IDPs by regressing out common covariates, including sex, age, age-squared, assessment center, standing height, and the first 20 genetic principal components (PCs). We then calculated pairwise correlations between the corrected IDPs. The left panel of Figure 2a shows the phenotypic correlations among vascular IDPs of the brain, carotid, and aorta. The total volume of WMH was positively correlated with the carotid IMT, the LD, and the aortic areas, but negatively correlated with the aortic

distensibilities. IDPs related to aortic areas and distensibilities showed strong positive correlations between the ascending and descending aorta, respectively, but were negatively correlated with each other. These measures were at best weakly correlated with the carotid IMT. However, a similar pattern was observed when correlating with carotid LD, with stronger signals compared to those seen with IMT, despite having a much smaller sample size (see Suppl. Figure 3).

The right panel of Figure 2a displays correlations between these IDPs and selected retinal vascular IDPs. The strongest positive correlations were found between the distensibility of both the ascending and descending aorta and the arteriolar retinal vessel diameter measurements (both the median across all segments and the retinal equivalent, which is specific to the largest retinal blood vessels). In contrast, the aortic areas were negatively correlated with these retinal IDPs and, to a lesser extent, with retinal arteriolar vascular density. Notably, retinal arteriolar vascular density was the only retinal IDP significantly correlated with the carotid IMT and LD. We also observed significant correlations between WMH and several retinal IDPs, with the strongest negative correlation seen with arteriolar median diameter and, somewhat weaker but still significant, with arteriolar retinal equivalent. Additionally, arteriolar tortuosity was negatively correlated with the area of the descending aorta. For more details, see Supplementary Text "Main vascular IDPs selection", and Supplementary Figure 3, which shows the number of subjects available for each IDP pair.

Since blood pressure is a critical factor influencing vascular properties globally [31, 32], we recomputed the pairwise correlations after also adjusting for hypertension (see Figure 2b). This additional adjustment reduced the magnitude of inter-IDP correlations overall, but did not affect the sign of any sizable correlation, apart from the IMT. Despite this reduction, the retinal arteriolar vessel diameter measures remained significantly positively correlated with the aortic distensibility and negatively with the area of the ascending aorta. Similarly, the negative correlation between the area of the descending aorta and arteriolar tortuosity persisted. However, the small but highly significant correlation between carotid IMT and aortic IDPs became insignificant. For further details, see Supplementary Data 'Phenotypic correlation'.

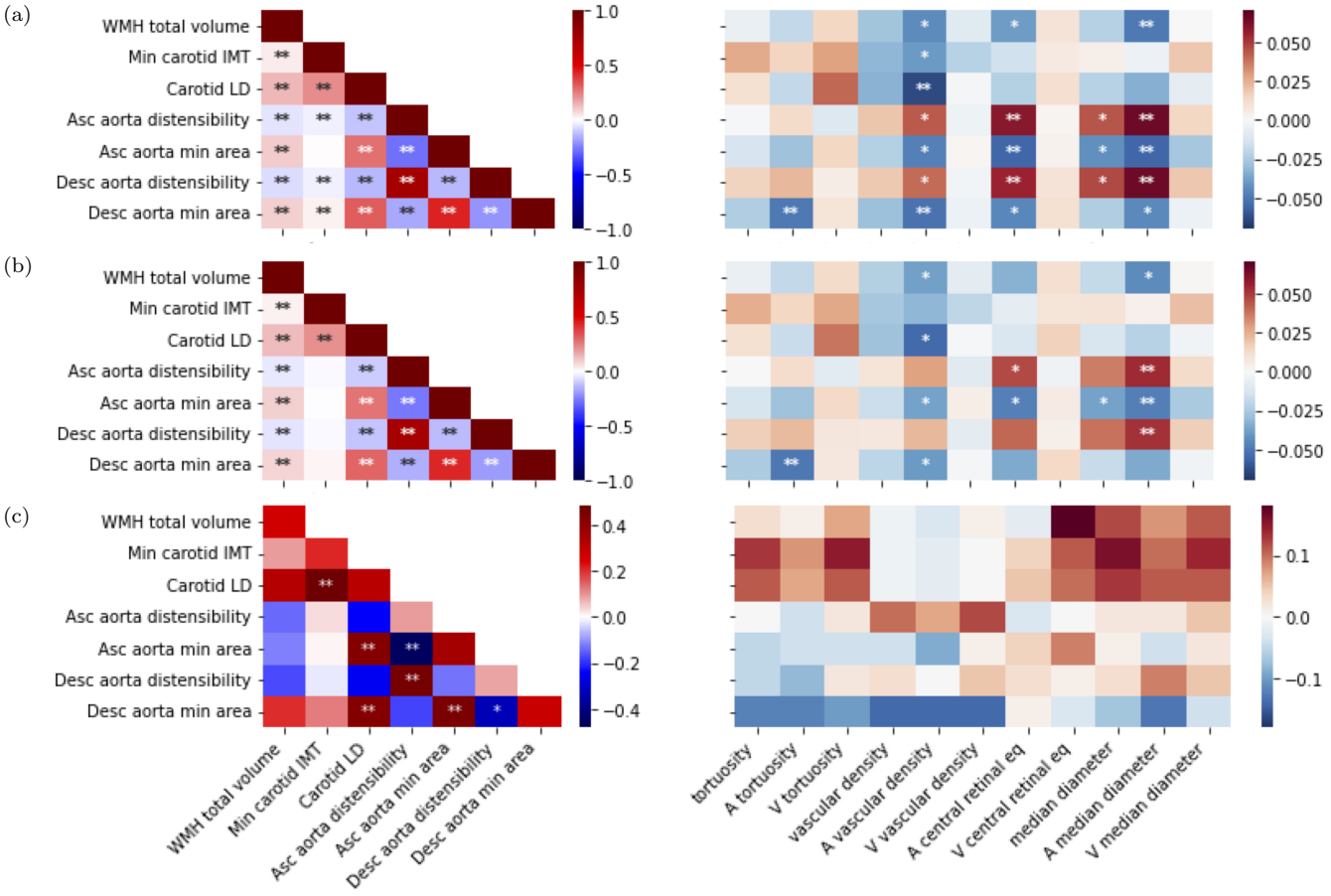

Figure 2: **a)** Phenotypic correlation of non-retinal IDPs with non-retinal IDPs (**left**) and retinal IDPs (**right**). **b)** Phenotypic correlation of non-retinal IDPs with non-retinal IDPs (**left**) and retinal IDPs (**right**) adjusted for hypertension in addition to the previous covariates. Hypertension was defined as having a systolic blood pressure (SBP) $\geq$ 140 mmHg or diastolic blood pressure (DBP) $\geq$ 90 mmHg. **c)** Genetic correlation of non-retinal IDPs with non-retinal IDPs (**left**) and retinal IDPs (**right**), computed using LDSR [33]. The diagonal of the left figure shows the heritability values of the non-retinal IDPs (values can be found in Supplementary Data 'Heritabilities'). GWAS summary statistics from previous studies were used to conduct this analysis (see section 4), for the brain IDPs, the GWAS sample size used was around ∼33,000 participants, for IMT around ∼44,000, for aortic IDPs $\in$ (33,000-38,000), and retinal IDPs $\in$ (54,000-69,000). For all the images, the x-axis shows non-retinal IDPs (**left**) and retinal IDPs (**right**) and the y-axis shows non-retinal IDPs. Colors indicate standardized effect sizes for linear regressions (a, b) or the genetic correlation coefficient (c), while asterisks indicate the level of statistical significance (except for the diagonal of Figure c). These p-values were corrected for multiple testing ($* : p < 0.05/N_{test}$, $** : p < 0.001/N_{test}$, where $N_{test} = N_{IDPs} \times (N_{IDPs}/2 + N_{retina})$). All IDPs were adjusted for covariates (see section 4). For more details, see Supplementary Data 'Main IDPs information'.

Next, we computed cross-IDP genetic correlations and SNP-heritabilities (h^2) using Linkage Disequilibrium Score Regression (LDSR) [33, 34], leveraging GWAS summary statistics from previous studies (see section 4). We observed significant genetic correlations exclusively between IDPs of the same organ (see left panel of Figure 2c, where h^2 are displayed on the diagonal). Specifically, the cross-sectional areas of the ascending and descending aorta were positively correlated with each other and negatively with the distensibilities.

Furthermore, carotid LD was possitively correlated with IMT, as well as with the ascending and descending cross-sectional areas of the aorta. Correcting for multiple hypotheses testing, no significant genetic correlation was found between these IDPs and retinal vascular IDPs (see right panel of Figure 2c). For more details on summary statistics, refer to the methods section 4.4, and Supplementary Data 'Main IDPs information', 'Genetic correlation', 'Heritabilities' for the values.

2.2 Genes and pathways associated with vascular IDPs

To identify genes associated with the IDPs, we used the *PascalX* analysis tool [35, 36]. The number of genes associated with non-retinal IDPs tended to be larger for IDPs with higher h^2 (see Figure 3a, left, diagonal). The IDPs with the most associated genes were the area of the ascending aorta ($h^2 = 0.36$, 157 genes) and the carotid IMT ($h^2 = 0.21$, 97 genes). The descending aorta ($h^2 = 0.28$, 90 genes) had fewer associated genes than its ascending counterpart. Distensibilities had much less associated genes, yet again more for the ascending ($h^2 = 0.09$, 12 genes) than the descending aorta ($h^2 = 0.08$, 7 genes). We also observed a large number of associated genes for WMH ($h^2 = 0.26$, 85 genes). The off-diagonal elements show the number of common genes for each pair of non-retinal IDPs. No single gene was shared among all non-retinal IDPs. WMH shared 22 genes with IMT, 18 with LD, and 11 with the ascending aorta area. IMT shared 32 genes with LD, 27 genes with the area of the ascending and 6 with the area of the descending aorta. Additionally, the respective genes associated with identical IDPs for the descending and ascending aorta displayed some overlap. The venular central retinal equivalent shared genes with WMH, IMT, LD, and the areas of the ascending and descending aorta (Figure 3a, right), including genes like *FBN1*, *CAPN12*, *EIF3K* and *SH2B3*. Retinal vascular densities shared genes with the descending aorta area, while tortuosities shared genes with WMH, IMT, LD, and the areas of the ascending and descending aorta, including genes like *SMAD3*, *COL4A1*, and *COL4A2*. For more details, see Supplementary Data 'Shared genes', and 'Heritabilities'.

We also used *PascalX* to identify annotated gene-sets (aka "pathways") enriched with high-scoring genes [35, 36]. The number of pathways associated with each IDP is shown in Figure 3b, left, diagonal. Specifically, ascending (36) and descending aorta minimum area (18) had the most associated pathways, and were the only IDPs with shared pathways (4), including the '*GO HEART DEVELOPMENT*' pathway. These IDPs also had the largest pathway overlap with retinal IDPs (Figure 3b, right), primarily with the tortuosity-related IDPs. The venular central retinal equivalent shared one gene set with IMT and LD, specifically a gene cluster on '*chr8p23*'. Vascular density shared one pathway with the ascending aorta minimum area, while tortuosities shared pathways with WMH and the areas of the aorta, including pathways like '*MANNO MIDBRAIN NEUROTYPES HENDO*', '*HP ABNORMAL VASCULAR MORPHOLOGY*', and actin-related ones, like '*GO ACTIN FILAMENT BUNDLE*', and '*GO ACTIN BINDING*'. For more details, see Supplementary Data 'Shared pathways'.

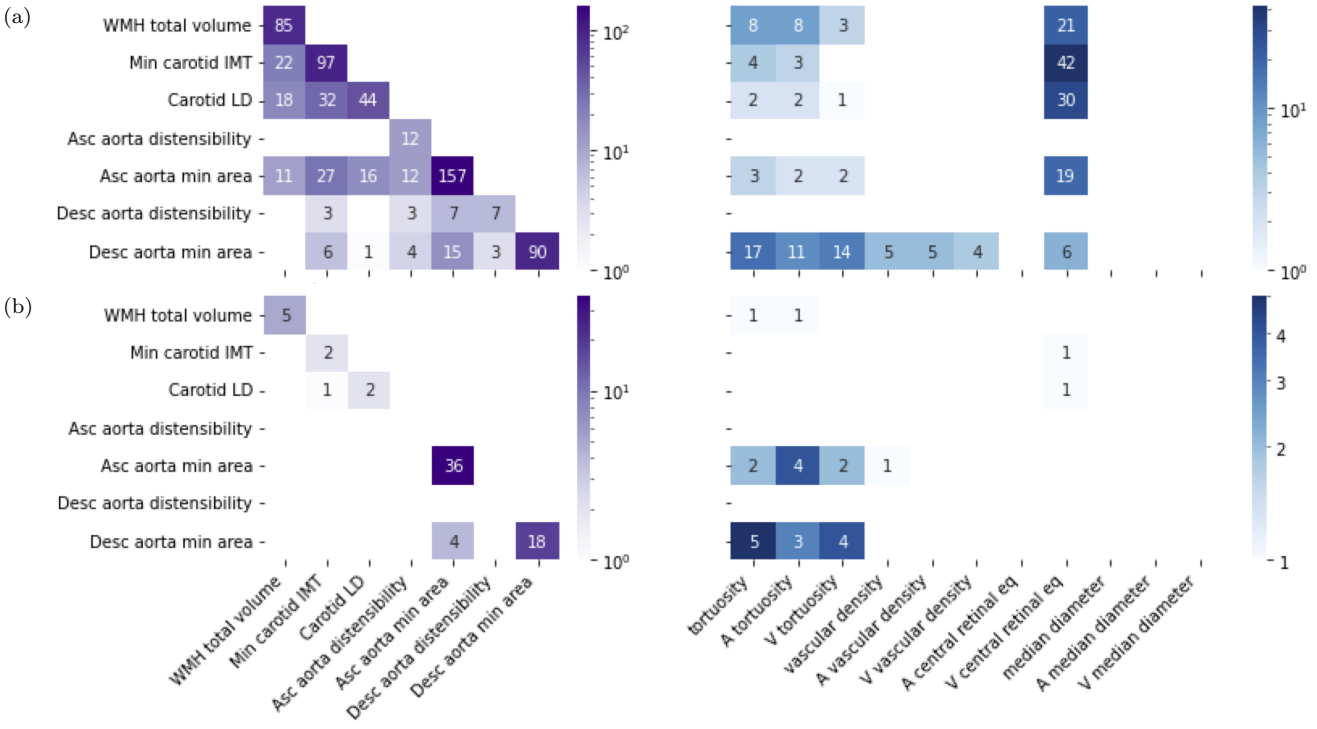

Figure 3: **a)** Gene-scoring intersection showing genes in common between non-retinal IDPs and non-retinal IDPs (**left**), and between non-retinal IDPs and retinal-IDPs (**right**). The diagonal (**left**) shows the number of genes significantly associated with each IDP. While the other cells show the number of intersected genes in IDP pairs. **b)** Pathway-scoring intersection showing pathways in common between non-retinal IDPs and non-retinal IDPs (**left**), and between non-retinal IDPs and retinal-IDPs (**right**). The diagonal (**left**) shows the number of pathways significantly associated with each IDP. While the other cells show the number of pathways in the intersection between pairs of IDPs. Genes and pathways results were obtained using *PascalX* [36].

3 Discussion and conclusions

In this study, we aimed to explore the associations between morphological vascular phenotypes within and across different organs. By leveraging the extensive imaging data from the UKB, we conducted an analysis that included IDPs from the brain, carotid, aortic arteries, and the retina. This comprehensive approach enabled us to discover numerous significant correlations both at the phenotypic and genotypic level.

From our previous work with IDPs measured from retinal CFIs [30], we observed that morphological IDPs in the retina were often correlated. In this study, we found that distensibility and cross-sectional area, measured in both the ascending and descending aorta, were negatively correlated. This negative correlation was observed both within the same anatomical region (e.g., ascending aorta) and across different regions (between the ascending and descending aorta). This can be attributed to the definition of distensibility, which is defined as the difference between the maximum and minimum cross-sectional areas divided by the product of the minimum area and the difference between the maximum and minimum pressures [23]. So,

this observed anti-correlation between distensibility and cross-sectional area is likely because, for a saturated difference, distensibility scales inversely to the area.

We observed multiple significant cross-organ correlations between vascular IDPs. For instance, the positive association between WMH and IMT (and LD), which aligns with previous studies that found an association between increased carotid IMT and a greater burden of cerebral WM lesions [37, 38]. Additionally, the negative correlations between carotid IMT (and LD) and lower aortic distensibilities are consistent with prior research, as both IDPs have been associated with a higher risk of heart failure [39, 40]. Our findings also confirmed previous observations that a greater WMH volume is associated with larger aortas (both descending and ascending) [41] and reduced aortic distensibility [16]. Conversely, WMH is associated with smaller diameters and reduced vascular density in the retinal arterioles. It is important to note that in the UKB, carotid ultrasound and brain and heart MRIs were typically conducted much later than retinal CFIs (median delay is about 9 years), suggesting that increased WMH volume arose subsequently to a reduction in the retinal microvasculature. However, to establish causality, longitudinal data from both imaging modalities would be necessary.

The associations of retinal vascular IDPs with those of the carotid, aorta, and WMH, highlight the potential of the retina as a non-invasive window into systemic vascular health. The negative association between retinal arteriolar vascular density and IMT, LD, and aortic areas, along with positive associations with aortic distensibility, emphasizes the complex interplay between retinal and other systemic vascular properties. This suggests that lower vascular density in the retina might reflect systemic vascular changes, such as increased IMT and larger aortic areas, which are indicative of vascular aging or pathology [42–45]. Conversely, higher aortic distensibility, which reflects healthier and more elastic arteries [46, 47], is associated with higher retinal vascular density. The retina, being a microvascular bed, might thus mirror microvascular health throughout the body, which is impacted by changes in large vessels like the aorta, or responds to microvascular disease. It is noteworthy that, despite the much smaller sample size, the phenotypic and genetic correlations of IMT and LD with the other IDPs followed similar patterns, but the correlations for LD were considerably stronger. The fact that many significant cross-organ phenotypic correlations were either absent or much weaker at the genetic level suggests that they are likely driven by environmental factors, including lifestyle. In contrast, within a single organ, there was mostly a strong alignment between phenotypic and genotypic correlations, indicating that the environmental impact is less pronounced in this case. Nevertheless, the shared associated genes between WMH, IMT, the aorta, and the retinal vascular IDPs indicate some common genetic underpinnings, with genes like *EIF3K*, *COL4A2*, and *SMAD3* [Gene Card] making them interesting candidates for modulators of systemic vascular health. Furthermore, the identification of shared pathways among retinal and aortic IDPs underscores the interconnected genetic mechanisms influencing vascular conditions across different organs.

The generalisability of our findings is limited by the specificity of the IDPs studied and the population characteristics of the UKB cohort. While compelling, these results may not fully translate to diverse populations or those with different health profiles. Practical limitations also include the resolution constraints of

non-invasive imaging modalities and the potential for selection bias in the UKB cohort. Our study primarily focused on genetic and phenotypic correlations, which can only serve as a starting point to elucidate the mechanistic pathways driving them. Future research should aim to validate our findings in more diverse populations and explore the mechanistic pathways underlying the observed associations.

Our study provides initial insight into the relationships between vascular morphology at different scales, from the microvasculature (as reflected in retinal IDPs and WMH as a marker of small vessel health) to the macrovasculature (properties of the aorta and carotid). This understanding can enhance our knowledge of systemic connections between various vasculatures and aid in the development of better prognostic tools for non-retinal vascular diseases using non-invasive, cost-effective retinal imaging.

4 Methods

4.1 The UKB Imaging Study

The UKB is a large-scale biomedical database and research resource containing anonymized genetic, lifestyle, and health information from half a million UK participants. The UKB's database, which includes blood samples, heart and brain scans, and genetic data of the volunteer participants, is globally accessible to approved researchers who are undertaking health-related research that's in the public interest. UKB recruited 500,000 people aged between 40-69 years in 2006-2010 from across the UK. With their consent, they provided detailed information about their lifestyle, physical measures and had blood, urine, and saliva samples collected and stored for future analysis. It includes multi-organ imaging for many participants, such as MRI scans of the brain, heart, and liver, carotid ultrasounds, and retinal CFIs [48].

The brain imaging data, covers six modalities: T1-weighted structural MRI, T2 FLAIR (fluid-attenuated inversion recovery), susceptibility-weighted MRI, resting-state functional MRI, task functional MRI, and diffusion MRI. These modalities yield various [49], including: a) Mean cerebral blood flow (CBF) maps, derived from arterial spin labeling (ASL) perfusion MRI, they provide insights into resting cerebral blood flow across the brain. b) Mean arterial transit time (ATT) maps, also from ASL data, and they indicate the time it takes for blood to travel from the neck to a given region of interest, potentially revealing vascular issues. Measures of mean CBF and ATT are available for each brain region. c) WMH volumes, obtained from T2 FLAIR structural MRI scans, they serve as markers for cerebral small vessel disease. The mean intensity and the volume of vessels are obtained from T1-weighted brain MRI using the Freesurfer automatic subcortical segmentation (ASEG) tool, for the right and left hemispheres ('Brain Imaging Documentation'*). Carotid ultrasound data, available for around 20,000 participants, was collected to measure carotid IMT, a marker for subclinical atherosclerosis and cardiovascular disease risk. Images were acquired from both left and right carotid arteries using standardized protocols across all assessment centers. Measurements were taken at four angles (120°, 150°, 210°, and 240°) around the carotid bulb. For each angle, the maximum,

*chrome-extension://efaidnbmnnnibpcajpcglclefindmkaj/https://biobank.ctsu.ox.ac.uk/crystal/crystal/docs/brain_mri.pdf

mean, and minimum IMT values were computed ('Carotid Ultrasound Documentation'[†]). It is important to note that IMT values were available for more subjects than the carotid images themselves.

Cardiovascular MRIs were acquired on 1.5T Siemens MAGNETOM Aera scanners. The imaging protocol included several sequences: Bright blood anatomical imaging in sagittal, coronal, and transverse planes; cine imaging of the left and right ventricles in both long-axis and short-axis views; myocardial tagging for strain analysis; native T1 mapping; aortic flow quantification; and imaging of the thoracic aorta [50]. This comprehensive protocol allows for detailed evaluation of aortic structure and function, providing (among others) IDPs related to aortic distensibility and dimensions. Aortic distensibility, which reflects aortic stiffness, was measured directly by the relative change in aortic cross-sectional area per unit change in pressure (lower distensibility signifies increased stiffness). Additionally, a variety of aortic dimension measures, including maximum and minimum areas, mean and standard deviation areas during diastole and systole, and mean absolute deviation, capture the dynamic changes in the cross-sectional areas of the ascending and descending aorta throughout the cardiac cycle [23–26].

Retinal CFIs, available for around 90,000 participants, were acquired from both eyes using a Topcon 3D OCT 1000 Mark II camera, with images centered to include both the optic disc and macula within a 45° field-of-view.

4.2 Main IDPs selection

We identified imaging modalities capable of capturing vascular morphology and determining relevant vascular IDPs. This process involved a thorough search across the UKB database, Google Scholar, and the GWAS catalog, using general vasculature-related keywords (e.g., 'vessel', 'vascular', 'vasculature', 'blood', 'artery', 'arterial', 'arterioral', 'vein', 'venular') and specific vessel names (e.g., 'carotid', 'aorta'). While our search aimed to capture all morphological vascular IDPs within the UKB dataset, we also found additional vascular IDPs in external sources that, despite being measured on the UKB dataset, were not yet available in the dataset (see Supplementary Data 'IDPs information' for details).

In the initial selection, we focused on organ-specific geometric and functional images without simplification. For the brain, IDPs such as CBF and ATT were available for all brain parts. To manage the high correlation among these measures, we calculated the average of CBF and ATT across the brain. We also considered total/deep/and peri-ventricular WMH volumes, as well as the mean intensity and volume of vessels in the brain, for both hemispheres (see Supplementary Figures 1 and 2). As explained before, carotid IMT IDPs were measured at four different angles, and for each, the main, minimum, and maximum values were available. These values were averaged across angles for consistency with previous studies. For heart vascular IDPs, we included various measures of ascending and descending areas, systolic and diastolic parameters, standard deviation, mean absolute deviation, stroke, and ejection fraction (see Supplementary Figure 2).

Further simplification was applied while ensuring the comprehensive representation of all organ images

[†] chrome-extension://efaidnbmnnnibpcajpcglclefindmkaj/https://biobank.ctsu.ox.ac.uk/crystal/ukb/docs/carult_explan_doc.pdf

vascular morphology. For the brain, although CBF and ATT are valuable for understanding associations among brain IDPs, they were not used as main IDPs due to their limited sample size and their potentially functional nature. Among the three WMH IDPs, only the total WMH was selected because of its strong correlations with other IDPs. We only considered WMH as a main vascular IDP for the brain, although data for total volume and intensity of a brain region annotated as 'vessels' (from FreeSurfer automatic segmentation of T1 images) were available. However, the number of voxels typically attributed to these regions was extremely small, and the corresponding IDPs did not correlate significantly with any of the other IDPs we studied (see Supplementary Figure 2). This suggests they may, at best, be very noisy representations of vascular entities. In contrast, WMH is a well-established marker of vascular lesions associated with small vessel disease [51].

For the carotid artery, only the minimum IMT was chosen due to its strong correlation with other measures. For the heart, we selected the minimum areas and distensibilities of the ascending and descending aorta because of their relevance and high correlations with other IDPs.

Finally, for retinal vascular IDPs, we aimed to ensure consistency with other morphological vascular IDPs, selecting only vascular density, tortuosity, and vessel diameters to comprehensively represent vascular morphology across different organs and systems.

4.3 Phenotypic correlation

For retinal IDPs, we used data from instance 0, which corresponds to the initial assessment visit (2006-2010) when participants were recruited and consent given, and instance 1, which corresponds to the first repeat assessment visit (2012-13). These IDPs were z-scored and adjusted for various covariates, including sex, age, age-squared, sex-by-age, sex-by-age-squared, spherical power, spherical power-squared, cylindrical power, cylindrical power-squared, instance, assessment center, genotype measurement batch, and genetic PCs 1-20 [30].

For the non-retinal vascular IDPs, only instances 2 (imaging visit, 2014+) and 3 (first repeat imaging visit, 2019+) were available. We used instance 2 due to its larger sample size, as fewer than 300 individuals per IDP were added if we included instance 3. Outliers in the retinal IDPs were already removed using a threshold of 10std [30]. The same criterion was applied to the non-retinal IDPs. These IDPs were also z-scored and adjusted for covariates, including age attended ('21003-2'), age attended squared, sex ('31'), UKB assessment center ('54'), standing height ('50-2'), and genetic PCs 1-20 ('22009-0.1' to '22009-0.20'). Similarly for LD [22].

We then reduced the selected non-retinal IDPs as detailed in section 4.2. After obtaining the residuals for all IDPs, we performed phenotypic correlation analysis using Pearson's correlation coefficient. Multiple testing correction was applied using the formulas: $* : p < 0.05/N_{test}$, $** : p < 0.001/N_{test}$, where $N_{test} = N_{IDPs} \times (N_{IDPs}/2 + N_{retina})$.

For the main non-retinal IDPs, the sample sizes and demographics were as follows:

IDP	Sample Size	Mean Age (y)	Std Age (y)	Female/Male
WMH total volume	40,302	64.0	7.7	1.11
Min carotid IMT	49,282	64.5	7.8	1.07
Carotid LD	18,808	64.0	7.6	1.03
Asc aorta distensibility	32,962	63.6	7.5	1.05
Asc aorta min area	36,120	63.6	7.6	1.06
Desc aorta distensibility	32,970	63.6	7.5	1.05
Desc aorta min area	36,121	63.6	7.6	1.06

Table 1: Demographic details and sample sizes for main non-retinal IDPs: Sample size (number of participants), mean age (in years), standard deviation of age (in years), and the female-to-male ratio for the main non-retinal IDPs.

4.4 Genetic correlation

To analyze genetic correlations for the main vascular IDPs, we accessed published GWAS summary statistics from the UKB. For the brain, we used summary statistics for the total volume of WMH, adjusted for covariates such as age, age-squared, sex, sex-by-age, sex-by-age-squared, 10 genetic PCs, head size, head position in the scanner, scanner table position, assessment center location, and date of attending assessment center. The sample size for these statistics was approximately 33,000 participants [52], 'Brain summary statistics'.

For the carotid minimum IMT, summary statistics were adjusted for the covariates: age at the time of the imaging visit, sex, genotyping array, and 30 genetic PCs, with a sample size of around 44,000 participants [53]. Summary statistics for the ascending and descending aorta distensibility and minimum areas were available in [23], 'Aorta summary statistics', using *bolt_P_BOLT_LMM_INF*. Retina summary statistics used the same covariates as those applied in the phenotypic analysis [30], 'Retina summary statistics'. And similarly for the carotid LDLD [22]. More information about the main IDPs can be found in Supplementary Data 'Main IDPs information'.

Genetic correlations and h^2 were computed using LDSR. Detailed results for h^2 can be found in Supplementary Data 'Heritabilities'). LDSR was also used to derive the genetic correlations between IDPs [33, 34].

4.5 Genes and pathways

Gene and pathway scores were computed using *PascalX* [36, 54]. Both protein-coding genes and lincRNAs were scored using the novel, approximate "saddle" method, taking into account all SNPs within a 50kb window around each gene. All pathways available in MSigDB v7.2 were scored using *PascalX*' ranking mode, fusing and rescoring any co-occurring genes less than 100kb apart. *PascalX* requires LD structure to accurately compute gene scores, which in our analyses was provided with the UK10K (hg19) reference

panel. Correction for bias due to sample overlap was done using the intercept from pairwise LDSR genetic correlation. The significance threshold was set at 0.05 divided by the number of tested genes (RANKING).

Data and code availability

Phenotypic data from the UKB are available upon application through the UKB website: https://www.ukbiobank.ac.uk. GWAS summary statistics can be accessed via the links provided in the document. The code for this study is available on the public GitHub repository: https://github.com/BergmannLab/multiorgan_vascular_IDPs.

Acknowledgements

The authors thank Leah Böttger, Olga Trofimova, David Presby, and Dennis Bontempi for their insightful comments on the manuscript. We also extend our gratitude to the study participants and the staff of the UKB, as well as the researchers who measured the IDPs and made the GWAS summary statistics publicly available.

Funding: Supported by the Swiss National Science Foundation grant no. CRSII5_209510 for the "VascX" Sinergia project. The authors declare no conflicts of interest.

References

[1] Alaide Chieffo, Gennaro Giustino, Pietro Spagnolo, Vasileios F Panoulas, Matteo Montorfano, Azeem Latib, Filippo Figini, Eustachio Agricola, Chiara Gerli, Annalisa Franco, et al. Routine screening of coronary artery disease with computed tomographic coronary angiography in place of invasive coronary angiography in patients undergoing transcatheter aortic valve replacement. *Circulation: Cardiovascular Interventions*, 8(7):e002025, 2015.

[2] Yoko Kato, Bharath Ambale-Venkatesh, Yoshimori Kassai, Larry Kasuboski, Joanne Schuijf, Karan Kapoor, Shelton Caruthers, and Joao AC Lima. Non-contrast coronary magnetic resonance angiography: current frontiers and future horizons. *Magnetic Resonance Materials in Physics, Biology and Medicine*, 33:591–612, 2020.

[3] Louis Arnould, Fabrice Meriaudeau, Charles Guenancia, Clement Germanese, Cécile Delcourt, Ryo Kawasaki, Carol Y Cheung, Catherine Creuzot-Garcher, and Andrzej Grzybowski. Using artificial intelligence to analyse the retinal vascular network: the future of cardiovascular risk assessment based on oculomics? a narrative review. *Ophthalmology and therapy*, 12(2):657–674, 2023.

[4] Areti Triantafyllou, P Anyfanti, N Koletsos, A Malliora, S Lamprou, K Dipla, and E Gkaliagkousi. Clinical significance of altered vascular morphology and function in normotension. *Current Hypertension Reports*, 25(10):287–297, 2023.

[5] Marsha L Eigenbrodt, Rishi Sukhija, Kathryn M Rose, Richard E Tracy, David J Couper, Gregory W Evans, Zoran Bursac, and Jawahar L Mehta. Common carotid artery wall thickness and external diameter as predictors of prevalent and incident cardiac events in a large population study. *Cardiovascular ultrasound*, 5:1–11, 2007.

[6] Sanaz Sedaghat, Thomas T Van Sloten, Stéphane Laurent, Gérard M London, Bruno Pannier, Maryam Kavousi, Francesco Mattace-Raso, Oscar H Franco, Pierre Boutouyrie, M Arfan Ikram, et al. Common carotid artery diameter and risk of cardiovascular events and mortality: pooled analyses of four cohort studies. *Hypertension*, 72(1):85–92, 2018.

[7] Ertan Yetkin, Selcuk Ozturk, et al. Dilating vascular diseases: pathophysiology and clinical aspects. *International Journal of Vascular Medicine*, 2018, 2018.

[8] Catherine M Francis, Matthias E Futschik, Jian Huang, Wenjia Bai, Muralidharan Sargurupremraj, Alexander Teumer, Monique MB Breteler, Enrico Petretto, Amanda SR Ho, Philippe Amouyel, et al. Genome-wide associations of aortic distensibility suggest causality for aortic aneurysms and brain white matter hyperintensities. *Nature communications*, 13(1):4505, 2022.

[9] M Kamran Ikram, Yi Ting Ong, Carol Y Cheung, and Tien Y Wong. Retinal vascular caliber measurements: clinical significance, current knowledge and future perspectives. *Ophthalmologica*, 229(3): 125–136, 2013.

[10] Sara B Seidelmann, Brian Claggett, Paco E Bravo, Ankur Gupta, Hoshang Farhad, Barbara E Klein, Ronald Klein, Marcelo Di Carli, and Scott D Solomon. Retinal vessel calibers in predicting long-term cardiovascular outcomes: the atherosclerosis risk in communities study. *Circulation*, 134(18):1328–1338, 2016.

[11] M Kamran Ikram, Frank Jan De Jong, Ewoud J Van Dijk, Niels D Prins, Albert Hofman, Monique MB Breteler, and Paulus TVM De Jong. Retinal vessel diameters and cerebral small vessel disease: the rotterdam scan study. *Brain*, 129(1):182–188, 2006.

[12] Raviv Allon, Michael Aronov, Michael Belkin, Elad Maor, Michael Shechter, and Ido Didi Fabian. Retinal microvascular signs as screening and prognostic factors for cardiac disease: a systematic review of current evidence. *The American Journal of Medicine*, 134(1):36–47, 2021.

[13] Gerald Liew, Paul Mitchell, Elena Rochtchina, Tien Yin Wong, Wynne Hsu, Mong Li Lee, Alan Wainwright, and Jie Jin Wang. Fractal analysis of retinal microvasculature and coronary heart disease mortality. *European heart journal*, 32(4):422–429, 2011.

[14] Ryo Kawasaki, Ning Cheung, Jie Jin Wang, Ronald Klein, Barbara EK Klein, Mary Frances Cotch, A Richey Sharrett, Steven Shea, FM Amirul Islam, and Tien Y Wong. Retinal vessel diameters and risk of hypertension: the multiethnic study of atherosclerosis. *Journal of hypertension*, 27(12):2386, 2009.

[15] Jie Jin Wang, Paul Mitchell, Harry Leung, Elena Rochtchina, Tien Yin Wong, and Ronald Klein. Hypertensive retinal vessel wall signs in a general older population: the blue mountains eye study. *Hypertension*, 42(4):534–541, 2003.

[16] Celeste McCracken, Zahra Raisi-Estabragh, Michele Veldsman, Betty Raman, Andrea Dennis, Masud Husain, Thomas E Nichols, Steffen E Petersen, and Stefan Neubauer. Multi-organ imaging demonstrates the heart-brain-liver axis in uk biobank participants. *Nature Communications*, 13(1):7839, 2022.

[17] Abdulrahman Ismaiel and Dan L Dumitraşcu. Cardiovascular risk in fatty liver disease: the liver-heart axis—literature review. *Frontiers in Medicine*, 6:202, 2019.

[18] Andres Diaz-Pinto, Nishant Ravikumar, Rahman Attar, Avan Suinesiaputra, Yitian Zhao, Eylem Levelt, Erica Dall'Armellina, Marco Lorenzi, Qingyu Chen, Tiarnan DL Keenan, et al. Predicting myocardial infarction through retinal scans and minimal personal information. *Nature Machine Intelligence*, 4(1): 55–61, 2022.

[19] Yi Liu, Nicolas Basty, Brandon Whitcher, Jimmy D Bell, Elena P Sorokin, Nick van Bruggen, E Louise Thomas, and Madeleine Cule. Genetic architecture of 11 organ traits derived from abdominal mri using deep learning. *Elife*, 10:e65554, 2021.

[20] Cathie Sudlow, John Gallacher, Naomi Allen, Valerie Beral, Paul Burton, John Danesh, Paul Downey, Paul Elliott, Jane Green, Martin Landray, et al. Uk biobank: an open access resource for identifying the causes of a wide range of complex diseases of middle and old age. *PLoS medicine*, 12(3):e1001779, 2015.

[21] Clare Bycroft, Colin Freeman, Desislava Petkova, Gavin Band, Lloyd T Elliott, Kevin Sharp, Allan Motyer, Damjan Vukcevic, Olivier Delaneau, Jared O'Connell, et al. The uk biobank resource with deep phenotyping and genomic data. *Nature*, 562(7726):203–209, 2018.

[22] Sofia Ortin Vela, Dennis Bontempi, Bianca Mazini, Leah Bottger, Olga Trofimova, and Sven Bergmann. Genetic insights from automated lumen diameter measurements in carotid ultrasounds of the uk biobank. *medRxiv*, 2025. doi: 10.1101/2025.01.07.25320106. URL https://www.medrxiv.org/content/early/2025/01/07/2025.01.07.25320106.

[23] Wenjia Bai, Hideaki Suzuki, Jian Huang, Catherine Francis, Shuo Wang, Giacomo Tarroni, Florian Guitton, Nay Aung, Kenneth Fung, Steffen E Petersen, et al. A population-based phenome-wide association study of cardiac and aortic structure and function. *Nature medicine*, 26(10):1654–1662, 2020.

[24] Steffen E Petersen, Nay Aung, Mihir M Sanghvi, Filip Zemrak, Kenneth Fung, Jose Miguel Paiva, Jane M Francis, Mohammed Y Khanji, Elena Lukaschuk, Aaron M Lee, et al. Reference ranges for cardiac structure and function using cardiovascular magnetic resonance (cmr) in caucasians from the uk biobank population cohort. *Journal of cardiovascular magnetic resonance*, 19(1):18, 2016.

[25] Luca Biasiolli, Evan Hann, Elena Lukaschuk, Valentina Carapella, Jose M Paiva, Nay Aung, Jennifer J Rayner, Konrad Werys, Kenneth Fung, Henrike Puchta, et al. Automated localization and quality control of the aorta in cine cmr can significantly accelerate processing of the uk biobank population data. *PLoS One*, 14(2):e0212272, 2019.

[26] Andrew Bard, Zahra Raisi-Estabragh, Maddalena Ardissino, Aaron Mark Lee, Francesca Pugliese, Damini Dey, Sandip Sarkar, Patricia B Munroe, Stefan Neubauer, Nicholas C Harvey, et al. Automated quality-controlled cardiovascular magnetic resonance pericardial fat quantification using a convolutional neural network in the uk biobank. *Frontiers in Cardiovascular Medicine*, 8:677574, 2021.

[27] Nay Aung, Jose D Vargas, Chaojie Yang, Kenneth Fung, Mihir M Sanghvi, Stefan K Piechnik, Stefan Neubauer, Ani Manichaikul, Jerome I Rotter, Kent D Taylor, et al. Genome-wide association analysis reveals insights into the genetic architecture of right ventricular structure and function. *Nature genetics*, 54(6):783–791, 2022.

[28] N Basty, EP Sorokin, M Thanaj, B Whitcher, Y Liu, JD Bell, EL Thomas, and M Cule. Cardiovascular measures from abdominal mri provide insights into abdominal vessel genetic architecture. 2022.

[29] Mattia Tomasoni, Michael Johannes Beyeler, Sofia Ortin Vela, Ninon Mounier, Eleonora Porcu, Tanguy Corre, Daniel Krefl, Alexander Luke Button, Hana Abouzeid, Konstantinidis Lazaros, et al. Genome-wide association studies of retinal vessel tortuosity identify numerous novel loci revealing genes and pathways associated with ocular and cardiometabolic diseases. *Ophthalmology Science*, 3(3):100288, 2023.

[30] Sofia Ortin Vela, Michael J Beyeler, Olga Trofimova, Ilaria Iuliani, Jose D Vargas Quiros, Victor A de Vries, Ilenia Meloni, Adham Elwakil, Florence Hoogewoud, Bart Liefers, et al. Phenotypic and genetic characteristics of retinal vascular parameters and their association with diseases. *medRxiv*, pages 2023–07, 2023.

[31] Michael K Pugsley and Reza Tabrizchi. The vascular system: An overview of structure and function. *Journal of pharmacological and toxicological methods*, 44(2):333–340, 2000.

[32] Hack-Lyoung Kim. Arterial stiffness and hypertension. *Clinical hypertension*, 29(1):31, 2023.

[33] Brendan K Bulik-Sullivan, Po-Ru Loh, Hilary K Finucane, Stephan Ripke, Jian Yang, Nick Patterson, Mark J Daly, Alkes L Price, and Benjamin M Neale. Ld score regression distinguishes confounding from polygenicity in genome-wide association studies. *Nature genetics*, 47(3):291–295, 2015.

[34] Brendan Bulik-Sullivan, Hilary K Finucane, Verneri Anttila, Alexander Gusev, Felix R Day, Po-Ru Loh, ReproGen Consortium, Psychiatric Genomics Consortium, Genetic Consortium for Anorexia Nervosa of the Wellcome Trust Case Control Consortium 3, Laramie Duncan, et al. An atlas of genetic correlations across human diseases and traits. *Nature genetics*, 47(11):1236–1241, 2015.

[35] David Lamparter, Daniel Marbach, Rico Rueedi, Zoltán Kutalik, and Sven Bergmann. Fast and rigorous computation of gene and pathway scores from snp-based summary statistics. *PLoS computational biology*, 12(1):e1004714, 2016.

[36] Daniel Krefl and Sven Bergmann. Cross-gwas coherence test at the gene and pathway level. *PLoS computational biology*, 18(9):e1010517, 2022.

[37] David Della-Morte, Chuanhui Dong, Matthew S Markert, Mitchell SV Elkind, Ralph L Sacco, Clinton B Wright, and Tatjana Rundek. Carotid intima-media thickness is associated with white matter hyperintensities: the northern manhattan study. *Stroke*, 49(2):304–311, 2018.

[38] Xin Chen, Yingqian Zhu, Shasha Geng, Qingqing Li, and Hua Jiang. Association of blood pressure variability and intima-media thickness with white matter hyperintensities in hypertensive patients. *Frontiers in Aging Neuroscience*, 11:192, 2019.

[39] Amer I Aladin, Elsayed Z Soliman, Dalane W Kitzman, Zeina Dardari, Shereen H Rasool, Joseph Yeboah, Matthew J Budoff, Bruce M Psaty, Pamela Ouyang, Joseph F Polak, et al. Comparison of the relation of carotid intima-media thickness with incident heart failure with reduced versus preserved ejection fraction (from the multi-ethnic study of atherosclerosis [mesa]). *The American journal of cardiology*, 148:102–109, 2021.

[40] Michael R Sood, Sahar S Abdelmoneim, Nripen Dontineni, Alexander Ivanov, Ernest Lee, Michael Rubin, Michael Vittoria, Marcella Meykler, Vidhya Ramachandran, Terrence Sacchi, et al. Descending aortic distensibility and cardiovascular outcomes: A cardiac magnetic resonance imaging study. *Vascular Health and Risk Management*, pages 653–665, 2022.

[41] Tatjana Rundek, David Della-Morte, Hannah Gardener, Chuanhui Dong, Matthew S Markert, Jose Gutierrez, Eugene Roberts, Mitchell SV Elkind, Charles DeCarli, Ralph L Sacco, et al. Relationship between carotid arterial properties and cerebral white matter hyperintensities. *Neurology*, 88(21):2036–2042, 2017.

[42] Samer S Najjar, Angelo Scuteri, and Edward G Lakatta. Arterial aging: is it an immutable cardiovascular risk factor? *Hypertension*, 46(3):454–462, 2005.

[43] Håkan Åstrand, Åsa Rydén-Ahlgren, Tomas Sandgren, and Toste Länne. Age-related increase in wall stress of the human abdominal aorta: an in vivo study. *Journal of vascular surgery*, 42(5):926–931, 2005.

[44] Michael R Skilton, David S Celermajer, Erich Cosmi, Fatima Crispi, Samuel S Gidding, Olli T Raitakari, and Elaine M Urbina. Natural history of atherosclerosis and abdominal aortic intima-media thickness: rationale, evidence, and best practice for detection of atherosclerosis in the young. *Journal of Clinical Medicine*, 8(8):1201, 2019.

[45] Luana de Rezende Mikael, Anelise Machado Gomes de Paiva, Marco Mota Gomes, Ana Luiza Lima Sousa, Paulo César Brandão Veiga Jardim, Priscila Valverde de Oliveira Vitorino, Maicon Borges Euzébio, Wátila de Moura Sousa, and Weimar Kunz Sebba Barroso. Vascular aging and arterial stiffness. *Arquivos brasileiros de cardiologia*, 109:253–258, 2017.

[46] Marina Cecelja, Bram Ruijsink, Esther Puyol-Antón, Ye Li, Harriet Godwin, Andrew P King, Reza Razavi, and Phil Chowienczyk. Aortic distensibility measured by automated analysis of magnetic resonance imaging predicts adverse cardiovascular events in uk biobank. *Journal of the American Heart Association*, 11(23):e026361, 2022.

[47] A Redheuil, C Wu, RT Yan, AG Bertoni, GW Hundley, DA Duprez, DR Jacobs, LB Daniels, DA Bluemke, and JAC Lima. Proximal aortic distensibility is an independent predictor of all-cause mortality and incident cardiovascular events in the multi-ethnic study of atherosclerosis. *European Heart Journal*, 34(suppl_1):2656, 2013.

[48] Thomas J Littlejohns, Jo Holliday, Lorna M Gibson, Steve Garratt, Niels Oesingmann, Fidel Alfaro-Almagro, Jimmy D Bell, Chris Boultwood, Rory Collins, Megan C Conroy, et al. The uk biobank imaging enhancement of 100,000 participants: rationale, data collection, management and future directions. *Nature communications*, 11(1):2624, 2020.

[49] Fidel Alfaro-Almagro, Mark Jenkinson, Neal K Bangerter, Jesper LR Andersson, Ludovica Griffanti, Gwenaëlle Douaud, Stamatios N Sotiropoulos, Saad Jbabdi, Moises Hernandez-Fernandez, Emmanuel Vallee, et al. Image processing and quality control for the first 10,000 brain imaging datasets from uk biobank. *Neuroimage*, 166:400–424, 2018.

[50] Zahra Raisi-Estabragh, Nicholas C Harvey, Stefan Neubauer, and Steffen E Petersen. Cardiovascular magnetic resonance imaging in the uk biobank: a major international health research resource. *European Heart Journal-Cardiovascular Imaging*, 22(3):251–258, 2021.

[51] Joanna M Wardlaw, Maria C Valdés Hernández, and Susana Muñoz-Maniega. What are white matter hyperintensities made of? relevance to vascular cognitive impairment. *Journal of the American Heart Association*, 4(6):e001140, 2015.

[52] Stephen M Smith, Gwenaëlle Douaud, Winfield Chen, Taylor Hanayik, Fidel Alfaro-Almagro, Kevin Sharp, and Lloyd T Elliott. An expanded set of genome-wide association studies of brain imaging phenotypes in uk biobank. *Nature neuroscience*, 24(5):737–745, 2021.

[53] Ming Wai Yeung, Siqi Wang, Yordi J van de Vegte, Oleg Borisov, Jessica van Setten, Harold Snieder, Niek Verweij, M Abdullah Said, and Pim van der Harst. Twenty-five novel loci for carotid intima-media thickness: a genome-wide association study in¿ 45 000 individuals and meta-analysis of¿ 100 000 individuals. *Arteriosclerosis, thrombosis, and vascular biology*, 42(4):484–501, 2022.

[54] Daniel Krefl, Alessandro Brandulas Cammarata, and Sven Bergmann. PascalX: a Python library for GWAS gene and pathway enrichment tests. *Bioinformatics*, 39(5):btad296, 05 2023. ISSN 1367-4811. doi: 10.1093/bioinformatics/btad296. URL https://doi.org/10.1093/bioinformatics/btad296.